land

MDPI

Article

Identification of the Spatio-Temporal Evolution Characteristics and Driving Factors of Ecosystem Service Supply and Demand in Typical Coal-Grain Overlapping Area, Eastern China

Qian Niu [1], Di Zhu [2], Yinghong Wang [3,*], Zhongyi Ding [1] and Guoqiang Qiu [4]

[1] School of Public Policy and Management, China University of Mining and Technology, Xuzhou 221116, China; tb20160027b4@cumt.edu.cn (Q.N.); dingzhongyi@cumt.edu.cn (Z.D.)
[2] School of Public Security Management, People's Public Security University of China, Beijing 100038, China; zhudi@ppsuc.edu.cn
[3] School of Environment Science and Spatial Informatics, China University of Mining and Technology, Xuzhou 221116, China
[4] College of Water Sciences, Beijing Normal University, Beijing 100875, China; qiuguoqiang@mail.bnu.edu.cn
* Correspondence: 1369@cumt.edu.cn; Tel.: +86-18115257389

Abstract

Investigating the spatio-temporal differentiation patterns and driving factors of ecosystem services (ESs) supply and demand is of great significance for early warning of ecosystem imbalance risks and identifying regional natural resource supply–demand conflicts. This study takes the typical coal-grain overlapping area (CGOA) in Eastern China as the research object, dividing it into mining townships (MT) and non-mining townships (NMT) for comparative analysis. By integrating the InVEST model, ESs supply–demand ratio (ESDR) index, four-quadrant model, and the XGBoost-SHAP algorithm, the study systematically reveals the spatiotemporal differentiation characteristics and driving mechanisms of ESs supply and demand from 2000 to 2020. The results indicated that: (1) grain production (GP) service maintained a continuous supply–demand surplus, with the ESDR of NMT areas surpassing that of MT areas in 2020. The ESDR of water yield (WY) service was significantly influenced by interannual fluctuations in supply, showing deficits in multiple years. The decline in carbon sequestration (CS) service and sharp increase in carbon emissions led to a continuous decrease in the ESDR of CS service, with MT areas facing a higher risk of carbon deficit. (2) The spatial heterogeneity of ESs supply and demand was significant, with GP and CS services exhibiting a typical urban-rural dual spatial structure, and the overall region was dominated by the Type II ESs supply–demand matching (ESDM) pattern. The ESDR of WY service generally decreases from Southeast to Northwest across the region. with the Type IV ESDM pattern dominating in most years. (3) Human activities are the core driving force shaping the supply–demand patterns of ESs. Among these, land use intensity exhibits a nonlinear effect, high population density demonstrates an inhibitory effect, and MT areas are more significantly affected by coal mining subsidence. Natural environmental factors primarily drive WY service. The research findings can provide a scientific reference for the coordinated allocation of regional natural resources and the sustainable development of the human–land system.

Keywords: ecosystem service supply and demand; XGBoost-SHAP; driving factors; InVEST model; coal-grain overlapping areas

Check for updates

Academic Editors: Lingzhi Wang, Yeting Fan and Hichem Omrani

Received: 25 November 2025
Revised: 11 January 2026
Accepted: 20 January 2026
Published: 22 January 2026

Copyright: © 2026 by the authors. Licensee MDPI, Basel, Switzerland. This article is an open access article distributed under the terms and conditions of the Creative Commons Attribution (CC BY) license.

1. Introduction

Since the "Anthropocene", the large-scale use of fossil energy has greatly improved productivity [1], and human activities have become the dominant driving force shaping the evolution of the Earth's surface system [2]. Meanwhile, urbanization, industrialization, and agricultural intensification have intensified the exploitation and utilization of natural resources [3], exerting tremendous pressure and disturbance on ecosystems. As revealed in the Millennium Ecosystem Assessment (MA) report, 60% of the ESs on which humans depend are currently in a state of decline, and nearly two-thirds of the world's natural resources are nearly depleted [4]. The Intergovernmental Science-Policy Platform on Biodiversity and Ecosystem Services (IPBES) Thematic Assessment Report on Land Degradation and Restoration also points out that 75% of the global terrestrial environments have been severely altered by human activities, with losses of ESs caused by land degradation exceeding 10% of the global gross product annually [5]. The United Nations' "Transforming Our World: The 2030 Agenda for Sustainable Development" identifies "protect, restore and promote the sustainable use of terrestrial ecosystems" as one of the 17 key sustainable development goals [6], highlighting the close connection between terrestrial ecosystems and human well-being.

ESs are the benefits provided by natural ecosystems through their structures and functions for human survival and development [7–9]. Among them, food security, water security, and addressing climate change are critical foundational environmental pillars for human survival and development [10]. However, with the acceleration of urbanization and industrialization, the demand for and reliance on the water–energy–food (WEF) nexus system in eastern China continue to rise [11]. Coupled with the demand preferences of diverse stakeholders, the resulting imbalances and prominent contradictions in the supply–demand relationships of ESs have become increasingly severe [12], particularly in populous resource-based regions [13]. CGOAs refer to a special geographic region where coal resource development and agricultural production overlap significantly in vertical space [14], leading to direct conflicts and coordinated governance needs between coal mining activities and grain production in terms of land use, ecological environment, and socioeconomic development [15,16]. The supply–demand relationship of ESs in the CGOAs is facing multiple pressures, including arable land shrinkage, water resource scarcity, and increasing risks of carbon deficit [17]. Behind this lies the combined stress of urban expansion, agricultural intensification, and mineral resource exploitation, yet current studies have neglected their complex driving mechanisms. Additionally, the cumulative effects of mineral resource development have led to structural contradictions and systemic degradation of the ecosystem in some areas, further exacerbating the imbalance between the supply and demand of ESs and the challenges to sustainable development in the CGOA. The Nansi Lake Basin, located in eastern China, boasts a history of agricultural development spanning thousands of years and a history of coal resource extraction exceeding a century. It is a typical plain CGOA; accordingly, the dual endowments of coal resources and arable land have laid a complex foundation for the supply–demand relationship of ESs in this region [18]. Therefore, clarifying the supply–demand relationships of ecosystem services and their complex driving mechanisms in this region is of paramount importance [19].

ES supply refers to the capacity of natural ecosystems to provide products and services for humans, while demand reflects human consumption, expectations, or preferences for ecosystem products and services [20–23]. The observed patterns of ES supply and demand reflect the long-term co-evolution of natural processes and human activities [24]. Assessment methods on the supply side are mature and diverse; early studies focused on evaluating the ecosystem services value (ESV) and later shifted to revealing ecological processes and mechanisms through ecological modeling. Among these, the InVEST model

holds advantages in comprehensive assessments due to its solid theoretical foundation, flexible modular design, and good universality [25–27], being widely applied in case studies across various regions, scales, and types. Models such as RUSLE, CASA, and SWAT are suitable for assessing specific individual services [28–30]. However, assessment methods on the demand side are scattered and underdeveloped, roughly divided into empirical cognition methods and indicator substitution methods. Empirical cognition methods, represented by the supply–demand matrix method and land use estimation method [20,31,32], are highly subjective, with excessively simplified data, parameters, and processes, making it difficult to capture ecological processes and details of supply–demand relationships. The basic paradigm of the indicator substitution method has gradually become clear through scholars' continuous empirical research and is increasingly widely used: first, select specific indicators characterizing service demand; second, calculate the total demand for services; finally, map the total demand to grid cells through spatial media [33–35]. Nevertheless, the indicator substitution method still lacks unified assessment standards, mainly due to the complexity of human activities and the heterogeneity of demands [24], as well as weak theoretical foundations and insufficient data support [23]. In practical research, it is necessary to adapt to local conditions when selecting applicable assessment methods and data indicators. Methods such as ESDR, spatial matching of supply and demand, and supply–demand coordination degree are usually used to measure and characterize the balance of ecosystem supply and demand [36,37], while methods like Moran's I and Self-Organizing Map (SOM) are employed to reveal their spatial agglomeration characteristics [38,39]. In most cases, there exist phenomena of spatial mismatch and quantitative imbalance in ES supply and demand [40], which have adverse impacts on human well-being and regional governance.

On the basis of revealing the supply–demand pattern, identifying key driving factors helps deepen the understanding of the evolution mechanism of ESs supply and demand, and also provides theoretical support for regional differentiated regulation [41]. The driving factors affecting the balance of ESs supply and demand mainly include two major aspects: the natural environment and socioeconomic factors [42]. Natural factors lay the foundation for ESs supply, while human activities indirectly affect the supply capacity of ESs by disturbing the components, structures, and processes of ecosystems [38]. The combination of different driving factors plays an important role in changing ESs supply and demand and shaping ESs relationships [43]. Previous studies have usually adopted methods such as Pearson correlation coefficient (PCC), Spearman's rank correlation coefficient (SRCC), Geographically weighted regression (GWR), Redundancy analysis (RDA), and Geographical detectors to identify the dominant driving factors of ESs evolution and their linear relationships [44,45]. However, these traditional methods still have obvious limitations in processing high-dimensional data, capturing nonlinear relationships, and analyzing threshold effects [46,47]. In recent years, with the rapid development of big data and artificial intelligence, machine learning algorithms such as Random Forest (RF) and Extreme Gradient Boosting (XGBoost) have been widely used in dynamic simulation, target optimization, and driving factor identification of complex systems due to their strong nonlinear fitting ability [48–50]. Nevertheless, as the complexity of machine learning model structures continues to increase, their decision-making process becomes disconnected from human cognitive logic, and the simulation results of the models are increasingly difficult to understand and interpret [51]. The SHAP (SHapley Additive exPlanations) interpretation method based on cooperative game theory effectively enables machine learning algorithms to break free from the "black box" dilemma by accurately analyzing the contribution mechanism of features in machine learning models [52,53]. The XGBoost-SHAP method is an analytical framework that deeply integrates XGBoost's strong predictive power with SHAP's interpretability [54]. It can meet the core needs of multi-factor coupling and non-

linear response in the research on driving factors of ESs and promote the transformation of ESs research from descriptive analysis to mechanistic interpretation.

This study takes the typical CGOA in the Nansi Lake Basin of Eastern China as the research region, the main research objectives are as follows: (1) Utilize the InVEST model and pixel matching method to explore the spatiotemporal variation patterns of ESs supply and demand; (2) Employ the ESDR index and four-quadrant model to investigate the balance of ESs supply and demand, as well as their ESDM status; (3) Integrate the XGBoost-Shap algorithm system to reveal the complex driving mechanisms underlying the spatial pattern of ESs supply and demand.

2. Study Area

The study area is a typical plain CGOA located in Eastern China and Southern North China Plain (115°40′–117°28′ E, 34°27′–35°58′ N), belonging to the Nansi Lake Basin, and is an important water resource division of the Yi-Shu-Si water system in the Huaihe River Basin. The administrative divisions encompass Jining City, Zaozhuang City, Heze City in Shandong Province, and Xuzhou City in Jiangsu Province, including 18 county-level administrative units with a total area of 20,317.64 km^2 (see Figure 1a,b). The region has a flat terrain, dense distribution of towns, and a large population. By 2023, the permanent population in the region reached 15.2827 million, with a population density of 752 people/km^2. Boasting fertile soil and developed agriculture, cultivated land accounts for more than 60% of the total area. Food crops such as winter wheat, corn, and soybeans are widely planted, and rice is also grown in some lakeside areas [55]. The region is rich in coal resources, with a total of 102 coal mines (68 of which are operating). All mines adopt the underground mining method, with an annual raw coal output exceeding 80 million tons. The coal seams in the mining areas are deeply buried, thick, and accompanied by a high groundwater table [56]. However, due to the coincidence of resource distribution, the phenomenon of cultivated land overlying coal resources is widespread. Long-term high-intensity mining has led to large-scale land subsidence and cultivated land loss. Based on the location of coal mines, mining area boundaries, degree of coal resource exploitation, and current status of coal mining subsidence areas, the CGOA is divided into 73 MT and 196 NMT with townships as the basic unit (see Figure 1c).

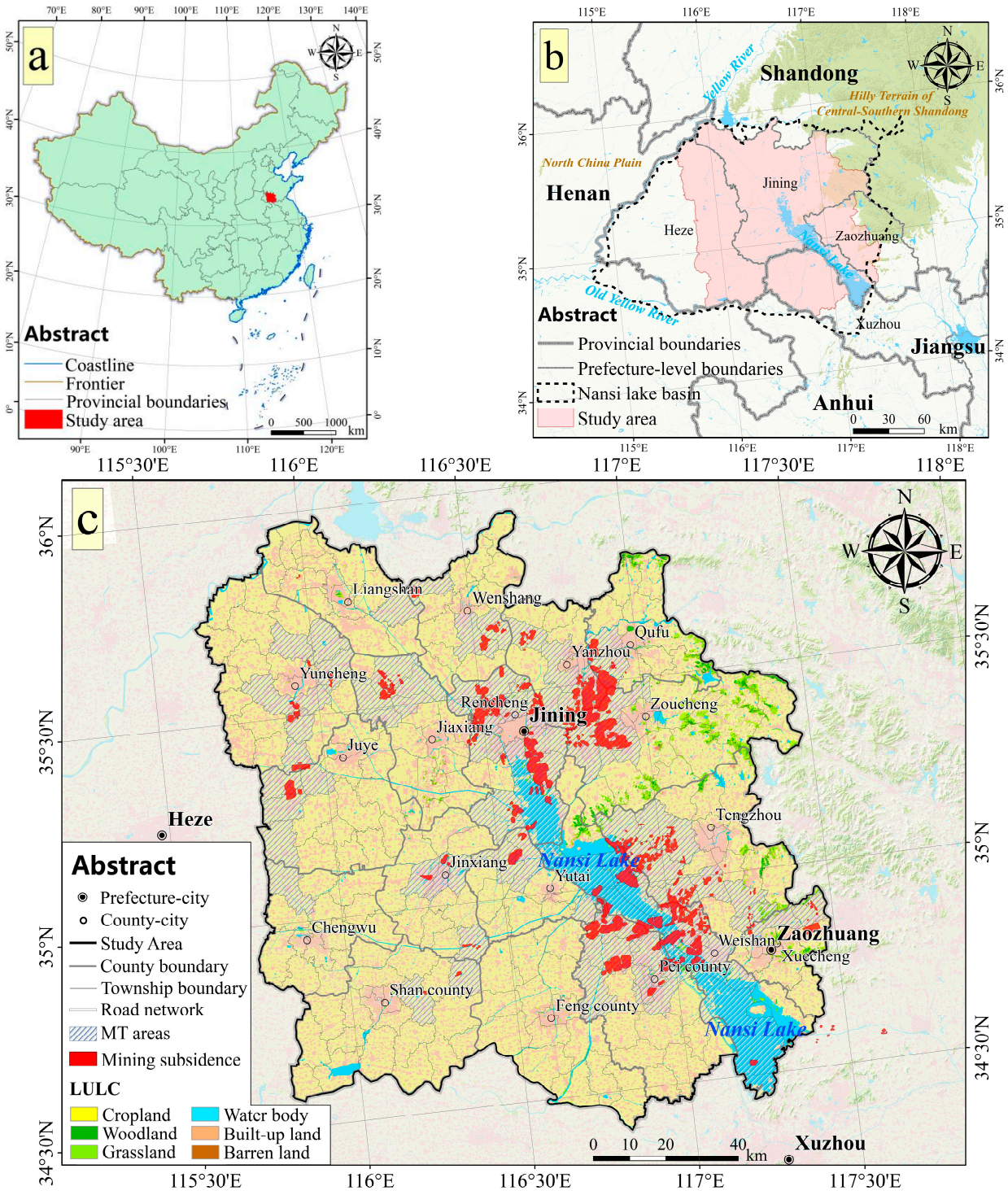


Figure 1. Location and scope of the study area: (**a**) the location of the research area in China; (**b**) the cross-administrative division situation of the study area and its inclusion relationship with the Nansi Lake Basin; (**c**) current land use/land cover (LULC) situation, current situation of coal mining subsidence areas, and the scope of the MT area.

3. Materials and Methods

3.1. Data Source

The data used in this study includes land use data, basic geographic data, socioeconomic data, and coalfield geological data. Table 1 details the content, time span, spatial resolution, and data sources of various types of data. All spatial data in this study were

obtained using the Albers Conical Equal Area projection coordinate system, GCSWGS_1984 geographic coordinate system, and the reference plane was D_WGS1984.

Table 1. Details of the data used in this study.

Data Type	Data Content	Data Year	Data Accuracy	Data Source
Land use data	Primary classification	2000–2020	30 m	CNLUCC (https://www.resdc.cn/Default.aspx, accessed on 22 September 2024)
Basic geographic data	DEM	2019	12.5 m	ALOS (https://search.asf.alaska.edu/, accessed on 14 November 2022)
	Soil data	2019	250 m	Predictive Soil Mapping with R. (https://opengeohub.org/)
	Meteorological data	1980–2020	-	National Meteorological Science Data Center (http://data.cma.cn/)
	NDVI	2000–2020	30 m	National Ecosystem Science Data Center (http://www.nesdc.org.cn/sdo/detail?id=60f68d757e28174f0e7d8d49, accessed on 12 February 2025)
Socio-economic data	GDP	2020	1 km	China's GDP Spatial Distribution Kilometer Grid Dataset (https://www.resdc.cn/Default.aspx)
	Population	2000–2020	100 m	WorldPop (https://hub.worldpop.org/project/categories?id=3, accessed on 2 February 2025)
	Road network data	2023	-	Open Street Map (https://www.openstreetmap.org/)
	Grain production statistics	2000–2022	-	The county-level agricultural product panel data
	Water resources statistics	2010–2024	-	Zaozhuang/Jining/Heze/Xuzhou (Urban and Rural) Water Affairs Bureau
	Carbon emission data	2000–2020	-	EDGAR GHG (https://edgar.jrc.ec.europa.eu/)
	Irrigated farmland ratio data	2020	250 m	CIrrMap250 Dataset (https://essd.copernicus.org/articles/16/5207/2024/essd-16-5207-2024.html, accessed on 26 July 2025)
Coalfield geological data	Mining boundary, coal mining subsidence area	2018	-	The First Exploration Team of the Shandong Coalfield Geologic Bureau

3.2. Methods

Figure 2 shows the technical roadmap. This roadmap revolves around the human environment system in the CGOA, and is developed in three steps: (1) Propose key scientific questions; (2) quantify the supply and demand of ESs and analyze their changing patterns, explore their quantitative balance status and spatial matching patterns; (3) considering natural environmental factors and human activity factors, analyze the importance and dependence of driving factors on the supply and demand of ESs.

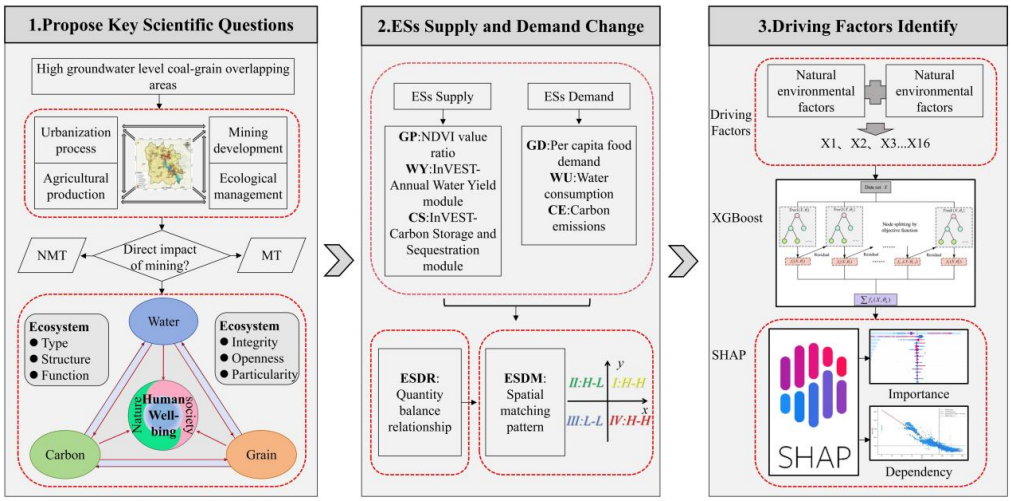


Figure 2. Research framework.

3.2.1. Quantification of Both Supply and Demand Sides

(1) Grain production service. Given the significant linear relationship between crop yield and NDVI [57], this study adopts the NDVI quota method to realize the spatialization of total GP, which is used to characterize the supply capacity of the ecosystem's food production service [34]. Grain demand (GD) is employed to represent the demand for food production services. Generally, grain demand includes grain for human consumption, feed grain, seed grain, industrial grain, and losses, but no subdivision is made in the calculation. The formulas are as follows:

$$GP = GP_{sum} \times \frac{NDVI_{ci}}{NDVI_{csum}} \quad (1)$$

$$GD = GD_{per} \times Pop_i \quad (2)$$

In the formula, GP denotes grain yield, GP_{sum} represents the total regional grain output, $NDVI_{ci}$ indicates the NDVI raster value of cultivated land, and $NDVI_{csum}$ denotes the total NDVI value of cultivated land. GD stands for grain demand, GD_{per} represents per capita grain demand, and Pop_i refers to the spatially rasterized population distribution.

(2) Water supply service. This study uses the Annual Water Yield module of the InVEST model to calculate water yield, which is used to characterize the supply capacity of the ecosystem's water supply service. Its basic principle is the Budyko hydrothermal balance equation, i.e., water yield equals the difference between precipitation and actual evapotranspiration [58]. Water use (WU) is adopted to represent the demand for water supply service, including farmland irrigation water use, forestry, fruit, livestock, and poultry water use, production and domestic water use, and ecological water supplement. Based on different land use types, the spatialization of total water use is realized by the NDVI quota method and the population density quota method, respectively. The formulas are as follows:

$$WY_i = \left(1 - \frac{AET_i}{P_i}\right) \times P_i \quad (3)$$

$$WU = WU_c \times \frac{NDVI_{ci}}{NDVI_{csum}} + WU_f \times \frac{NDVI_{fi}}{NDVI_{fsum}} + WU_p \times \frac{Pop_i}{Pop_{sum}} + \frac{WU_e}{wgrid_{sum}} \quad (4)$$

In the formula, WY_i denotes the raster-derived water yield, AET_i represents the raster-based actual evapotranspiration, and P_i indicates the raster-based precipitation. Detailed procedures and parameter principles are detailed in the InVEST model User's Guide and will not be repeated here. WU stands for water use, with WU_c, WU_f, WU_p, and WU_e

representing total irrigation water use for farmland, forestry and fruit crops, livestock and poultry, industrial and domestic water use, and ecological replenishment, respectively. $NDVI_{ci}$ and $NDVI_{wi}$ are the raster values of NDVI for cultivated land and forest/grassland, while $NDVI_{csum}$ and $NDVI_{fsum}$ denote their respective total values. Pop_i indicates the spatially distributed population raster, Pop_{sum} represents the total regional population, and $wgrid_{sum}$ denotes the number of water body rasters.

(3) Carbon sequestration service. This study uses the Carbon Storage and Sequestration module of the InVEST model to calculate carbon storage, which is used to characterize the supply capacity of the ecosystem's carbon sequestration service. A carbon density table is formulated with reference to relevant studies on the Nansi Lake Basin and Yanzhou Mining Area [59,60]. Carbon emissions (CE) are employed to represent the demand for carbon sequestration service, and the population quota method is used to realize the spatialization of total carbon emissions. The formulas are as follows:

$$C_{tot} = C_{above} + C_{below} + C_{soil} + C_{dead} \tag{5}$$

$$CE = CE_{sum} \times \frac{Pop_i}{Pop_{sum}} \tag{6}$$

In the formula, C_{tot} denotes the total carbon sequestration in terrestrial ecosystems, C_{above} represents carbon sequestration in above-ground components, C_{below} indicates carbon sequestration in below-ground components, C_{soil} stands for soil carbon sequestration, and C_{dead} refers to carbon sequestration in dead organic matter. CE_{sum} is the total regional carbon emissions, Pop_i denotes the spatial distribution of the population in raster format, and Pop_{sum} represents the total regional population.

3.2.2. Quantitative Matching Analysis: ESDR

The ESDR is a core indicator to measure the matching relationship between the supply capacity and the intensity of demand for ESs, which can reflect the balance state of supply and demand for ESs [61]. The calculation formula is as follows:

$$ESDR = \frac{ES - ED}{(ES_{\max} + ED_{\max}) \div 2} \tag{7}$$

In this formula, ESDR is defined as the ratio of ESs supply to demand, where ES represents the supply and ED the demand. $ESDR_{max}$ and $ESDR_{min}$ denote the maximum supply and demand levels, respectively. A positive ESDR indicates an oversupply (surplus), a negative ESDR indicates undersupply (deficit), while ESDR = 0 signifies equilibrium.

3.2.3. Spatial Matching Analysis: Based on the Four Quadrants Model

The four-quadrant model is introduced to reveal the ESDM pattern [62]. Its core logic involves: after applying Z-core standardization to both supply and demand quantities, a two-dimensional coordinate system is constructed with supply level (x-axis) and demand level (y-axis). By setting thresholds, spatial units are categorized into four quadrants: type I (high supply/high demand, spatial alignment), type II (high supply/low demand, spatial mismatch), type III (low supply/low demand, spatial alignment), and type IV (low supply/high demand, spatial mismatch). This classification enables analysis of spatial matching characteristics within each quadrant and identification of regions with prominent supply–demand conflicts. The Z-core standardization formula is:

$$Z = \frac{(x - \mu)}{\sigma} \tag{8}$$

In this formula, Z represents the standardized raster value of ESs supply and demand, x denotes the original raster value, μ is the mean, and σ is the standard deviation. Both μ and σ are available in the raster properties of ArcGIS10.2.

3.2.4. Driving Factor Analysis Based on XGBoost-SHAP

This section analyzes the driving factors of the ESDR in the CGOA using XGBoost-SHAP, which integrates the strong predictive power of XGBoost with the interpretability of SHAP values. First, the machine learning model captures complex driving mechanisms; then, the interpretation tool quantifies the contribution intensity and direction of each factor; finally, it reveals the underlying causes of the regional ESs supply–demand relationship [47,48,51]. Before constructing the XGBoost algorithm, it is necessary to test the independence among evaluation factors. High correlation among factors will seriously impair the scientific validity and accuracy of the model, so multicollinearity between factors should be avoided. The Pearson Correlation Coefficient (PCC) was adopted to preliminarily evaluate the correlation between driving factors, and the formula is given as follows.

$$PCC = \frac{Cov(X_i, X_j)}{\sigma(X_i)\sigma(X_j)} \tag{9}$$

In the formula, PCC refers to the Pearson correlation coefficient between factors; $Cov(X_i,Y_j)$ denotes the covariance between variable X_i and variable X_j; $\sigma(X_i)$, $\sigma(X_j)$ represent the standard deviations of variable X_i and variable Y_j, respectively. The value range of PCC is $(-1, 1)$. The positive or negative sign of the coefficient reflects the direction of the linear correlation between factors (positive or negative correlation), and the absolute value indicates the strength of the correlation. It is generally recognized that when ($|PCC| > 0.8$), there is a strong linear correlation between factors; when ($0.5 < |PCC| < 0.8$), the correlation is moderate; when ($|PCC| < 0.5$), the linear correlation between factors is weak, and the multicollinearity in this case is not significant enough to interfere with the model's identification of the independent effects of each factor.

XGBoost iteratively trains multiple weak decision trees (CART) to fit the residuals of previous models, ultimately achieving integrated strong predictive power. The objective function of XGBoost consists of two parts: the loss function and the regularization term.

$$Obj^{(t)} = \sum_{i=1}^{n} L\left(\hat{y}_i^{(t)}, y_i\right) + \sum_{m=1}^{t} \Omega(f_m) \tag{10}$$

In this formula, $\hat{y}^{(t)}$ denotes the predicted value of the i-th sample at the t-th step, L(*) represents the loss function, and $\Omega(f_m)$ is the regularization term for the m-th tree. XGBoost employs a forward stepwise algorithm, optimizing only the current tree ft at each step. By approximating the loss function with a second-order Taylor expansion, the objective function can be further simplified to:

$$Obj^{(t)} = \sum_{i=1}^{n} \left[g_i f_t(x_i) + \frac{1}{2} h_i f_t(x_i)_2 \right] + \Omega(f_t) \tag{11}$$

In this formula, g_i denotes the first derivative of the data point with respect to the loss function, while hi represents its second derivative.

SHAP leverages the Shapley value from cooperative game theory to quantify each feature's marginal contribution to predictions, thereby enhancing model interpretabil-

ity [54]. For a model with K features, the Shapley value φ_i of feature i represents its average marginal contribution across all possible feature subset combinations.

$$\varphi_i = \sum_{S \subseteq F \setminus \{i\}} \frac{|S|! \times (|F| - |S| - 1)!}{|F|!} [v(S \cup \{i\}) - v(S)] \quad (12)$$

In this formula, F denotes the complete set of features, S represents the subset excluding feature i, and $v(S)$ indicates the model's prediction output when using only subset S.

To improve model operation efficiency, the raster layers of these 16 driving factors were divided into 500 m × 500 m grids using the Fishnet tool in ArcGIS, and the raster values were extracted to the center points of the grids. Taking the GP_ESDR, WY_ESDR, and CS_ESDR as dependent variables, and the 16 driving factors as independent variables, XGBoost-SHAP analysis was implemented based on Python3.12. The maximum number of iterations was set to 30, and the dataset was split into a training set and a test set at a ratio of 7:3 to verify the model fitting performance. On this basis, a combined SHAP feature importance plot was generated to compare the differences in driving factors between MT and NMT areas, and to explore the driving mechanism of the ESs supply–demand pattern in CGOAs.

4. Results

4.1. Spatial-Temporal Variation Characteristics of ESs Supply and Demand

4.1.1. Analysis of the Spatio-Temporal Changes in the Supply and Demand Quantity of ESs

As can be seen from Figure 3, the GP, WY, and CS services in the region all exhibit strong spatial heterogeneity. The high-value areas of the GP service are distributed in the eastern and western parts of Nansi Lake and the Wensi concentrated farmland areas, where the terrain is flat, the soil is fertile, and the area of cultivated land is extensive. The low-value areas of GP services are primarily distributed in the Nansi Lake area, urban built-up areas, and the eastern mountainous areas, with scattered cultivated land and an expanding urban footprint. The spatial pattern of the WY service is greatly affected by the interannual variation in precipitation, showing an overall pattern of low in the northwest and high in the southeast, with the main high-value areas distributed in the eastern mountainous areas and urban built-up areas, and the low-value areas are mainly distributed in the Nansi Lake area and the northwestern corner of the region. The high-value areas of the CS service are scattered, mainly in the mountainous forest-grassland areas of the eastern part of the region; the medium-value areas are mainly cultivated land, with the widest distribution; and the low-value areas are urban built-up areas and the Nansi Lake area. A horizontal comparison of the spatial patterns of the three ESs reveals a certain degree of similarity; that is, the GP service, WY service, and CS service capacities in the Nansi Lake area and urban built-up areas are all in a weak state. A longitudinal comparison between 2000 and 2020 reveals that the low-value zones of GP and CS services and the high-value zones of WY service all expanded, showcasing a consistent pattern with urban sprawl.

As can be seen from Figure 4, the GD, WU, and CE in the region all exhibit strong spatial heterogeneity. The high-value areas of GD are mainly distributed in the built-up areas of cities and townships, while low-value areas are mainly located in the Nansi Lake area and the vast farmland areas. The high-value areas of WU are also mainly distributed in the built-up areas of cities and townships, the medium-value areas are mainly distributed in farmland areas, and the low-value areas are mainly in the Nansi Lake area. The spatial distribution pattern of CE is similar to that of grain demand, with high-value areas mainly concentrated in the built-up areas of cities and townships, as well as along major transportation routes, where residents' daily life, industrial production, and

motor vehicle use all emit large amounts of carbon dioxide. A longitudinal comparison from 2000 to 2020 shows that the high-value areas of the three service demands expanded, accompanied by a concomitant contraction of their low-value areas—a pattern that aligns with urban spatial expansion. Overall, the spatial patterns of GD, WU, and CE in the region share a certain similarity, that is, the high-value areas highly overlap with the core areas of human activities, which intuitively reflects the important driving role of human activities on the structure and function of ecosystems.

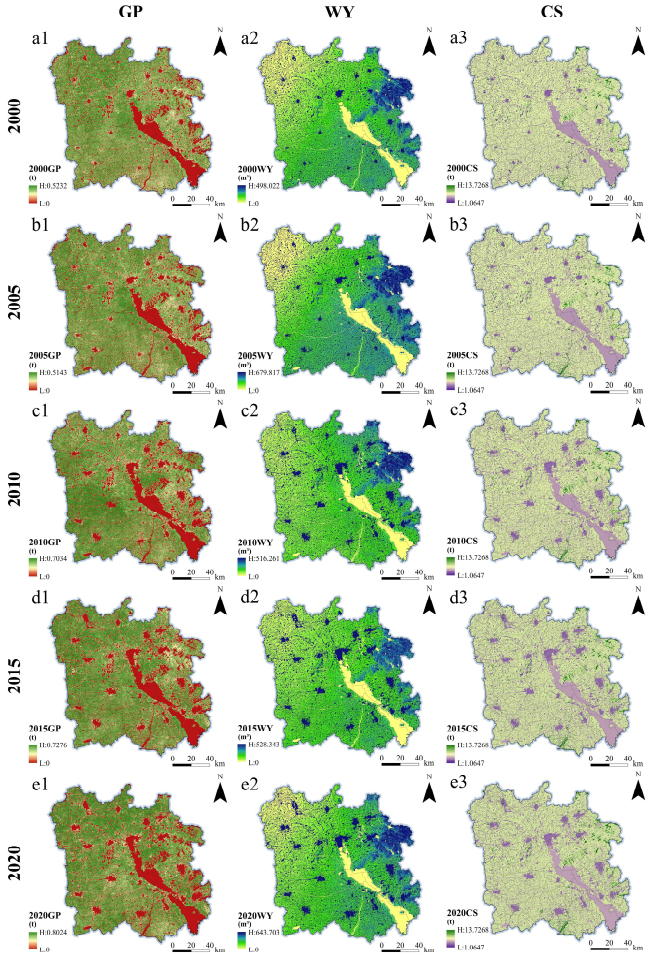


Figure 3. Spatial distribution of ESs supply from 2000 to 2020: (**a1**) 2000GP; (**a2**) 2000WY; (**a3**) 2000CS; (**b1**) 2005GP; (**b2**) 2005WY; (**b3**) 2005CS; (**c1**) 2010GP; (**c2**) 2010WY; (**c3**) 2010CS; (**d1**) 2015GP; (**d2**) 2015WY; (**d3**) 2015CS; (**e1**) 2020GP; (**e2**) 2020WY; (**e3**) 2020CS.

As shown in Figure 5, significant changes occurred in the supply and demand of GP, WY, and CS services within the region during the period 2000–2020. The total GP service increased from approximately 0.071 billion tons to about 0.10 billion tons, with the yield per unit area rising from 3.40 t/ha to 4.84 t/ha. Meanwhile, the total GD grew from about 0.053 billion tons to around 0.061 billion tons, and the demand per unit area was 3.13 t/ha in the NMT area and 2.25 t/ha in the MT area, indicating that the growth rate of production exceeded that of demand. WY service showed notable interannual fluctuations, with values of 3.29 billion m^3, 6.526 billion m^3, 4.33 billion m^3, 4.246 billion m^3, and 5.875 billion m^3 in 2000, 2005, 2010, 2015, and 2020, respectively. In contrast, WU decreased from 4.878 billion m^3 to 4.339 billion m^3 over the same period, reflecting improved water–use efficiency. CS service declined from about 1.95 billion tons to approximately 1.92 billion tons, resulting in a loss of over 0.02 billion tons of carbon sink over the 20 years. In contrast, CE surged from around 0.43 billion tons to about 1.31 billion tons, nearly tripling. For all

indicators, the intensity in the NMT area was higher than that in the MT area, including GP per unit area (4.34 vs. 3.70 t/ha), WY per unit area (2523.52 vs. 2112.86 m^3/ha), and CS per unit area (96.12 vs. 93.23 t/ha). Likewise, the intensities of demand and emissions were also more pronounced in the NMT area.

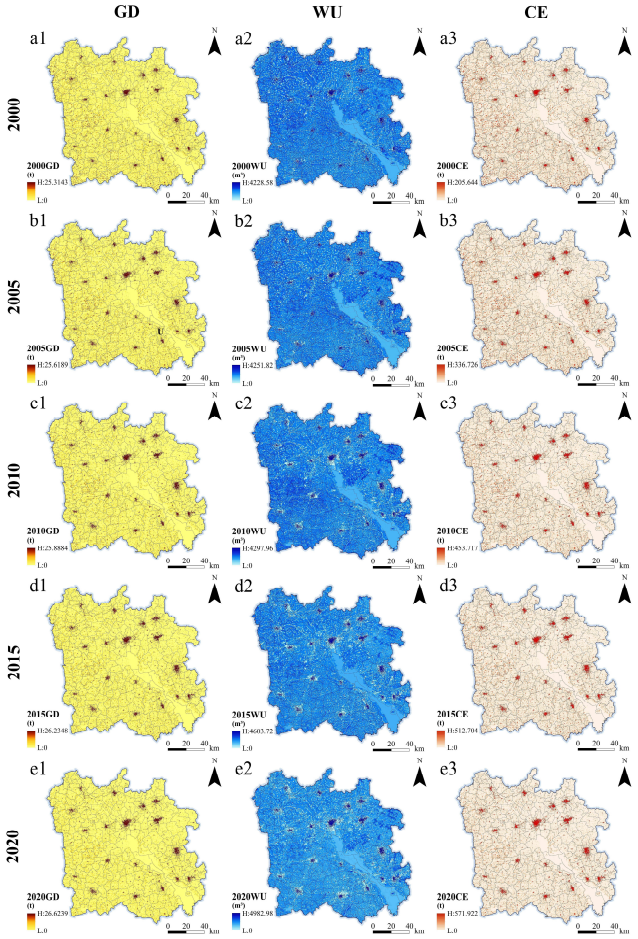


Figure 4. Spatial distribution of ESs demand from 2000 to 2020: (**a1**) 2000GD; (**a2**) 2000WU; (**a3**) 2000CE; (**b1**) 2005GD; (**b2**) 2005WU; (**b3**) 2005CE; (**c1**) 2010GD; (**c2**) 2010WU; (**c3**) 2010CE; (**d1**) 2015GD; (**d2**) 2015WU; (**d3**) 2015CE; (**e1**) 2020GD; (**e2**) 2020WU; (**e3**) 2020CE.

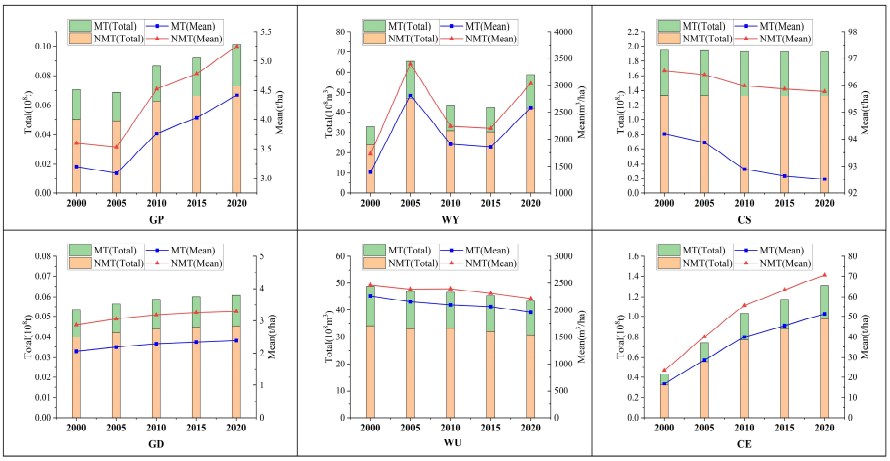


Figure 5. Changes and trends in ESs supply and demand from 2000 to 2020.

4.1.2. Analysis of Spatial-Temporal Variation in ESDR

As can be seen from Figure 6, the grain production ESDR (GP_ESDR), water yield ESDR (WY_ESDR), and carbon sequestration ESDR (CS_ESDR) all exhibit strong spatial heterogeneity, with significant changes in their spatial patterns over the years. The high-value areas of the GP_ESDR are in the concentrated farmland areas; the medium-value areas are in the Nansi Lake area and eastern mountainous areas; and the low-value areas are distributed in the built-up areas of various cities and towns. The spatial heterogeneity and interannual volatility of the WY_ESDR are more obvious, which is also related to the uneven interannual distribution of precipitation. The WY_ESDR is higher in the south than in the north, higher in the east than in the west, higher in mountainous areas than in plain and lake areas, and higher in urban centers than in suburbs and rural areas. In 2000, 2010, and 2015, the WY_ESDR in most areas was less than 0; in 2005, it was greater than 0 in most areas; and in 2020, the areas of high-value and low-value regions were roughly equal. The high-value areas of the CS_ESDR are mainly located in the eastern mountainous areas and concentrated farmland areas, which are the main sources of carbon sinks in the region; the medium-value areas are mainly distributed in the Nansi Lake area, the outskirts of cities and towns, and near rural residential areas, the low-value areas are distributed in the built-up areas of various cities and towns. From an overall perspective, the high-value zones of GP_ESDR expanded, whereas those of CS_ESDR contracted. Despite pronounced interannual variability in WY_ESDR, a persistent WY service deficit was maintained in the northwestern region.

As can be seen from Figure 7, during the period 2000–2020, the GP_ESDR, WY_ESDR, and CS_ESDR all underwent significant changes. The GP_ESDR has consistently maintained a surplus state where supply exceeds demand; except for a slight decrease in 2005, the ratio generally showed a continuous upward trend. It should be stressed that before 2015, the GP_ESDR of MT was higher than that of NMT, but NMT surpassed MT in 2020. The WY_ESDR fluctuated widely over the years, with supply deficits in 2000, 2010, and 2015, highlighting the dilemma of a regional surface water resource shortage. Additionally, the WY_ESDR of MT was lower than that of NMT. CS_ESDR has consistently maintained a surplus status, albeit showing a persistent decline that is now approaching the deficit threshold. Nevertheless, the rate of this decline has moderated. Simultaneously, the CS_ESDR of MT was higher than that of NMT.

4.1.3. Analysis of the Current Spatial Pattern of ESDM

As shown in Figure 8, the patterns of regional grain production ESDM (GP_ESDM), water yield ESDM (WY_ESDM), and carbon sequestration ESDM (CS_ESDM) exhibit spatial heterogeneity, with a pronounced spatial mismatch between supply and demand areas. GP_ESDM is predominantly characterized by Type II, which extensively covers non-urban agricultural regions. This is followed by Type III, mainly distributed in the Nansi Lake area and the eastern mountainous region. Type IV appears next, primarily located in multiple urban built-up areas. Type I covers the smallest and relatively most fragmented area, mostly around some rural settlements. WY_ESDM demonstrates more distinct spatial heterogeneity. Overall, the southeastern part of the region is dominated by Type I and Type II patterns. However, Type IV predominates in the western part. The spatial pattern of CS_ESDM is similar to that of GP_ESDM, with Type II being the most common. Type III is mainly distributed in the Nansi Lake area, while Type IV is primarily found in urban areas with intensive human production and living activities.

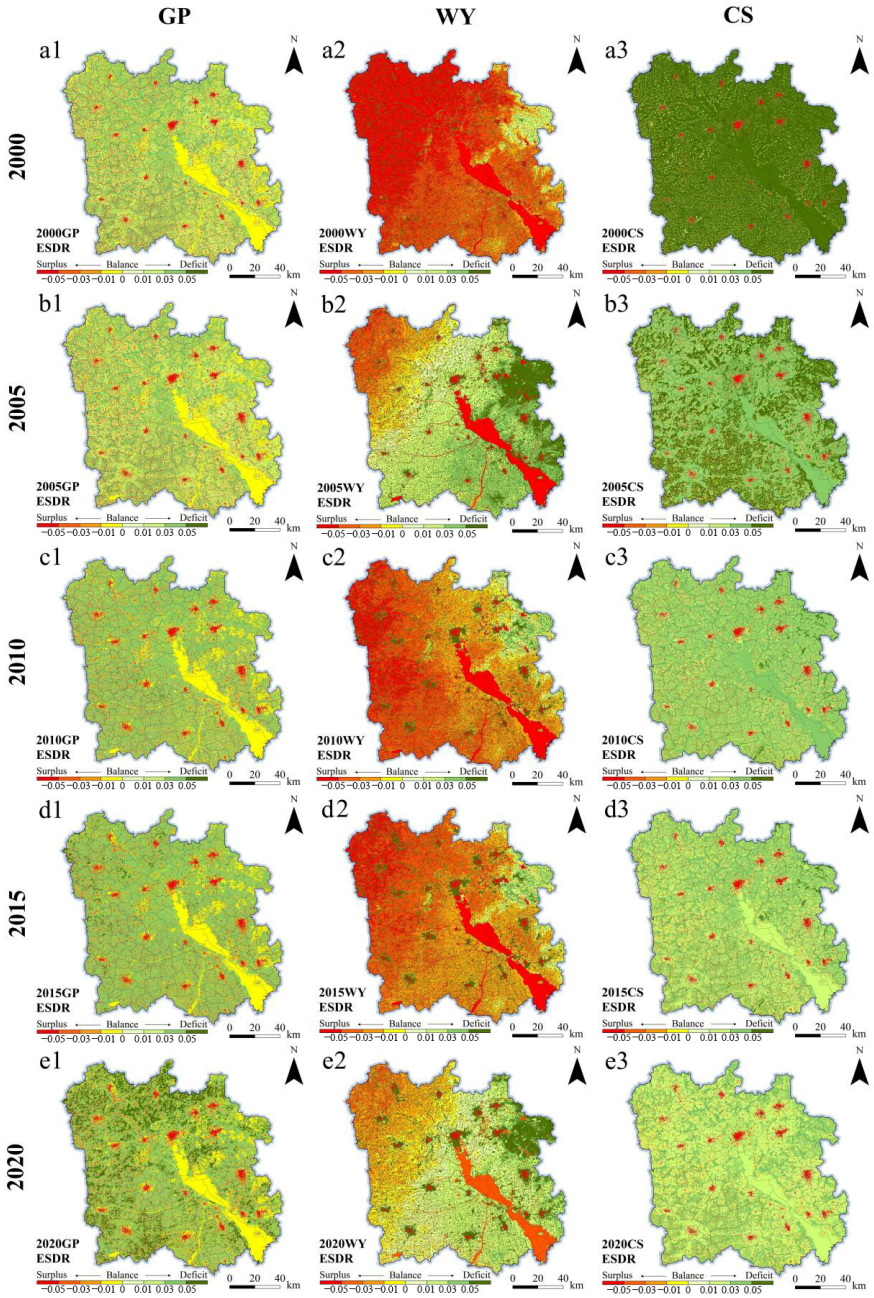


Figure 6. Spatial distribution of ESDR from 2000 to 2020: (**a1**) 2000GP_ESDR; (**a2**) 2000WY_ESDR; (**a3**) 2000CS_ESDR; (**b1**) 2005GP_ESDR; (**b2**) 2005WY_ESDR; (**b3**) 2005CS_ESDR; (**c1**) 2010GP_ESDR; (**c2**) 2010WY_ESDR; (**c3**) 2010CS_ESDR; (**d1**) 2015GP_ESDR; (**d2**) 2015WY_ESDR; (**d3**) 2015CS_ESDR; (**e1**) 2020GP_ESDR; (**e2**) 2020WY_ESDR; (**e3**) 2020CS_ESDR.

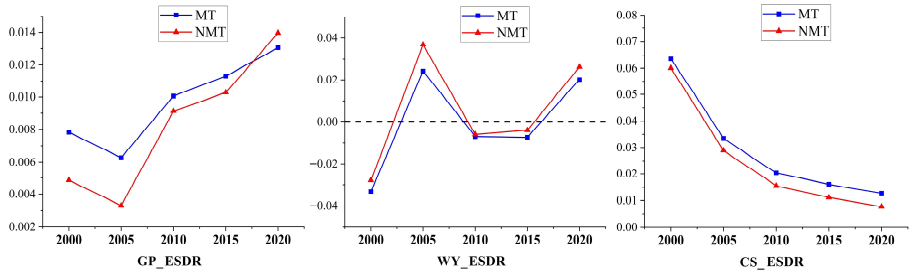


Figure 7. The changing trend of ESDR from 2000 to 2020.

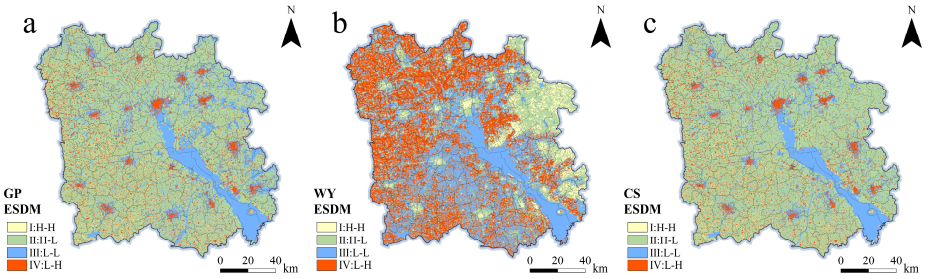


Figure 8. Spatial distribution of ESDM: (**a**) GP_ESDM; (**b**) WY_ESDM; (**c**) CS_ESDM.

Table 2 presents the proportional distribution of GP_ESDM, WY_ESDM, and CS_ESDM types. Overall, GP_ESDM and CS_ESDM are highly similar in structure. Both are dominated by Type II, accounting for 63.60% and 68.19%, respectively. Type I has the lowest proportion in both, each around 4%. The proportions of Type III and Type IV are also relatively close: Type III accounts for 22.78% and 18.19%, respectively, while Type IV accounts for less than 10% in both. In sharp contrast, WY shows a significantly different ESDM structure, with Type II accounting for only 22.04%, while Type III and Type IV have relatively higher proportions, together exceeding 70%.

Table 2. Proportions of various ESDM patterns in the entire region.

ESDM Type	GP_ESDM	WYESDM	CS_ESDM
I	4.05%	7.27%	4.39%
II	63.60%	22.04%	68.19%
III	22.78%	36.28%	18.19%
IV	9.57%	34.41%	9.23%

A double-ring proportional chart (Figure 9) is used to illustrate the similarities and differences in the ESDM quantity structure between the MT and NMT areas, with the inner ring representing the MT area and the outer ring representing the NMT area. Consistent with the overall regional pattern, the structures of GP_ESDM and CS_ESDM are highly similar in both MT and NMT, with Type II being the dominant pattern in each, accounting for over 50% in both areas. Additionally, WY_ESDM in both MT and NMT is primarily characterized by Type III and Type IV patterns. In terms of regional differences between MT and NMT, the proportion of Type III ESDM for all three ESs is higher in MT than in NMT. Conversely, the proportion of Type II for both GP_ESDM and CS_ESDM is higher in NMT than in MT, and the proportion of Type IV for WY_ESDM is also higher in NMT than in MT.

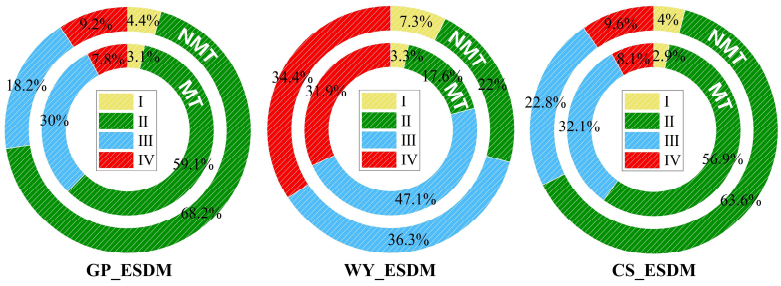


Figure 9. Proportions of ESDM patterns in MT and NMT regions.

4.2. Analysis of Driving Factors in the Supply and Demand Balance of ESs

4.2.1. Correlation Analysis of Driving Factors

The efficiency of ecosystems is regulated by multiple factors, including climate, geomorphology, land use, and socioeconomic activities. The supply–demand pattern of ESs in CGOAs is the result of the combined effects of the natural background and human activities. In this study, in accordance with the principles of scientific rigor, comprehensiveness, and data availability, and considering the balance between natural environment factors and human activity factors, 16 driving factors were systematically selected for analysis, including 8 natural environment factors and 8 human activity factors. Natural environment factors cover four aspects: topography, climate, soil, and vegetation. Among them, topographic factors include elevation (X1) and slope (X2); climatic factors include temperature (X3), precipitation (X4), and potential evapotranspiration (X5); soil factors include soil layer thickness (X6) and soil fertility (represented by organic matter content, X7); and vegetation factors include NDVI (X8). Human activity factors cover three aspects: urban expansion, agricultural production, and mineral resource development. Among them, urban expansion factors include land use intensity (X9), GDP (X10), night-time light (X11), road network density (X12), and population density (X13); agricultural production factors include the proportion of irrigated farmland (X14); and mineral resource development factors include coal mine density (X15) and coal mining subsidence area status (X16).

The correlation heatmap among driving factors was plotted using the corrplot package in R4.3.2. As shown in Figure 10, the absolute values of the correlations between X1 and X6, and between X10 and X11, are close to 0.5 but do not exceed the critical value; the absolute values of most other driving factors are below 0.3. Therefore, the evaluation factors selected in this study meet the correlation requirements and can all be used.

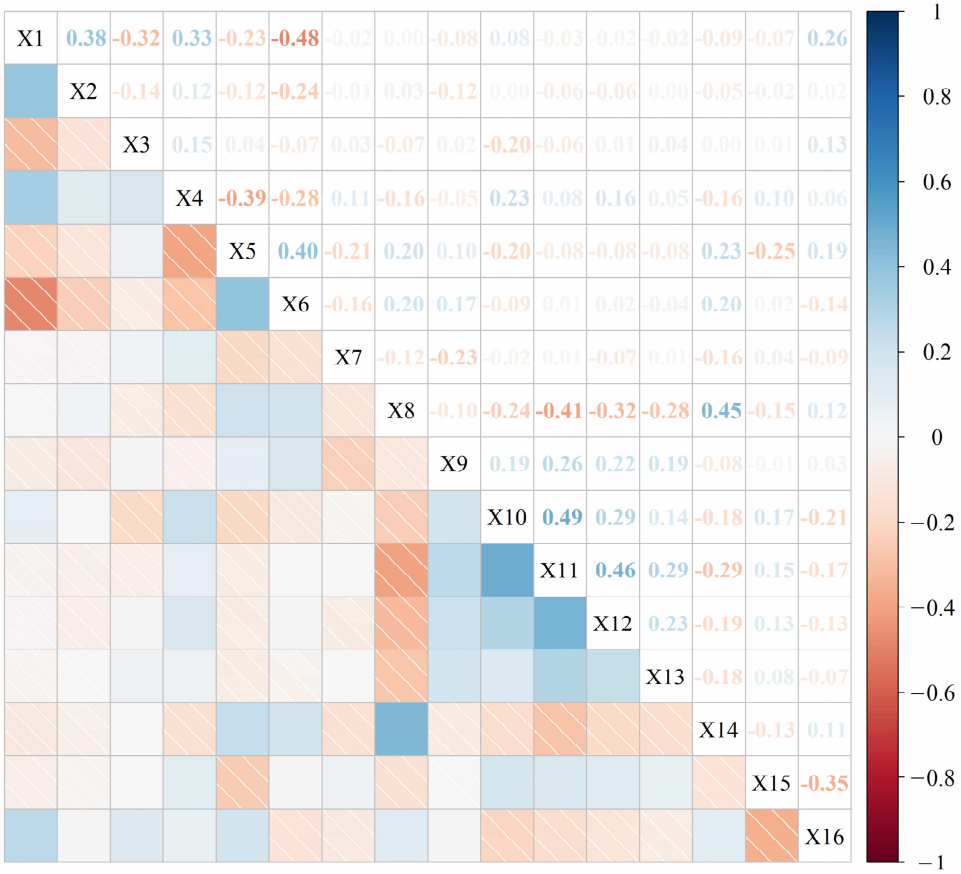


Figure 10. Driver factor Heatmap of Pearson correlation coefficients.

4.2.2. Importance Analysis of Driving Factors

As revealed by the XGBoost simulation results, the R^2 of all training sets exceeded 0.98, and the R^2 of all test sets exceeded 0.97. This indicates that the model achieved high accuracy on both the training and test sets, with no overfitting occurring, and exhibited excellent generalization ability. The trained XGBoost model demonstrated high accuracy and stability; thus, the subsequent SHAP value analysis using this model is highly reliable and suitable for analyzing the driving factors of ESs supply and demand patterns in CGOAs.

The combined SHAP feature importance plot can intuitively characterize the contribution degree and effect of all driving factors on the ESDR (Figure 11). In MT areas, factors such as X13 and X9 had the strongest importance: their contribution degrees to the GP_ESDR were 39.5% and 36.8%, respectively, to the WY_ESDR were 18.2% and 72.3%, respectively, and to the CS_ESDR were 81.2% and 12.4%, respectively. In NMT areas, X13 and X9 also had the strongest importance: their contribution degrees to the GP_ESDR were 51.6% and 33.8%, respectively, to the WY_ESDR were 22.4% and 54.4%, respectively, and to the CS_ESDR were 76.3% and 11.2%, respectively. From the overall contribution degree of the above driving factors, human activities are undoubtedly the dominant factors affecting the balance of ESs supply and demand. The impacts of natural environment factors and mineral resource development factors are relatively weak overall. Compared with the other two ESs, the WY_ESDR is more affected by natural environment factors, such as X4, X6, and X8. The influence of mineral resource development factors on the balance of ESs supply and demand in MT areas is stronger than that in NMT areas. Among these factors, the importance of X16 in GP, WY, and CS ranked 4th, 9th, and 5th, respectively.

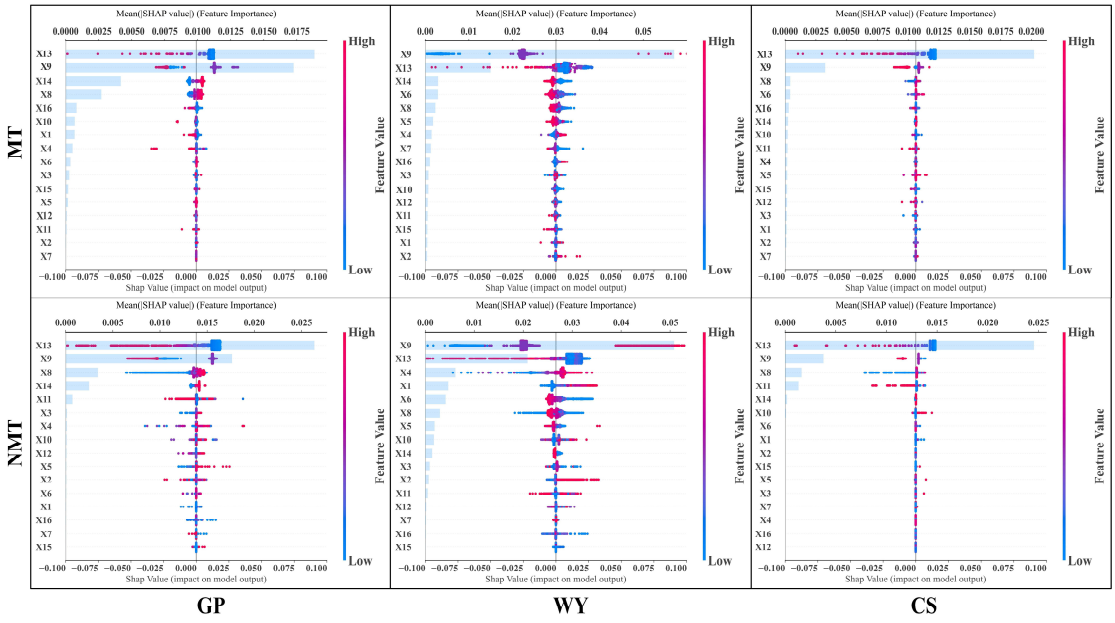


Figure 11. Driving factors of the ESs supply–demand relationship and their importance with SHAP combination charts.

After identifying the dominant driving factors of the ESs supply–demand pattern in CGOAs, the driving mechanism was further analyzed. Overall, low characteristic values of factors such as X9 and X13 are concentrated in the positive value region of SHAP, which indicates that low-intensity human activities can increase the ESDR. Correspondingly, high-intensity human activities exacerbate the imbalance between the supply and demand sides of ESs through population agglomeration, a surge in demand, and the reshaping of surface landscapes. In terms of GP service, whether in MT areas or NMT areas, the increase

in X8 and the X14 will improve their supply–demand balance; irrigation is an important factor ensuring the growth of food crops in arid farmlands in the region, while NDVI can accurately characterize the growth status of crops and directly act on the supply side of grain production. In WY service, high characteristic values of X4 are concentrated in the positive value region of SHAP, as the main source of surface runoff in the region, abundant precipitation can directly enhance water production capacity. In contrast, high characteristic values of factors such as X8 and X6 are concentrated in the negative value region of the dependent variable, and these factors reduce the supply of surface water resources by inhibiting runoff generation and increasing infiltration. In CS service, SHAP values of low NDVI are mostly negative, which reflects that vegetation serves as the core carrier of carbon sequestration; insufficient vegetation coverage will weaken carbon sequestration capacity, and vegetation destruction will directly lead to carbon sink loss. In addition, it is worth noting that in MT areas, X16 mainly acts on the supply side of GP, WY, and CS service. Coal mining subsidence areas in high phreatic level mining areas will form subsidence basins and subsidence waterlogging, and the loss of cultivated land, runoff, and carbon sinks will worsen the supply–demand imbalance.

4.2.3. Dependence Analysis of Driving Factors

The complex driving mechanism of the balance between supply and demand of ESs in CGOAs was analyzed using SHAP dependence plots of key driving factors. In this study, the top three key driving factors affecting the ESDR of each ES in the MT and NMT areas were selected, respectively, mainly including X9, X13, X14, X8, and X4, details are shown in Figures 12 and 13.

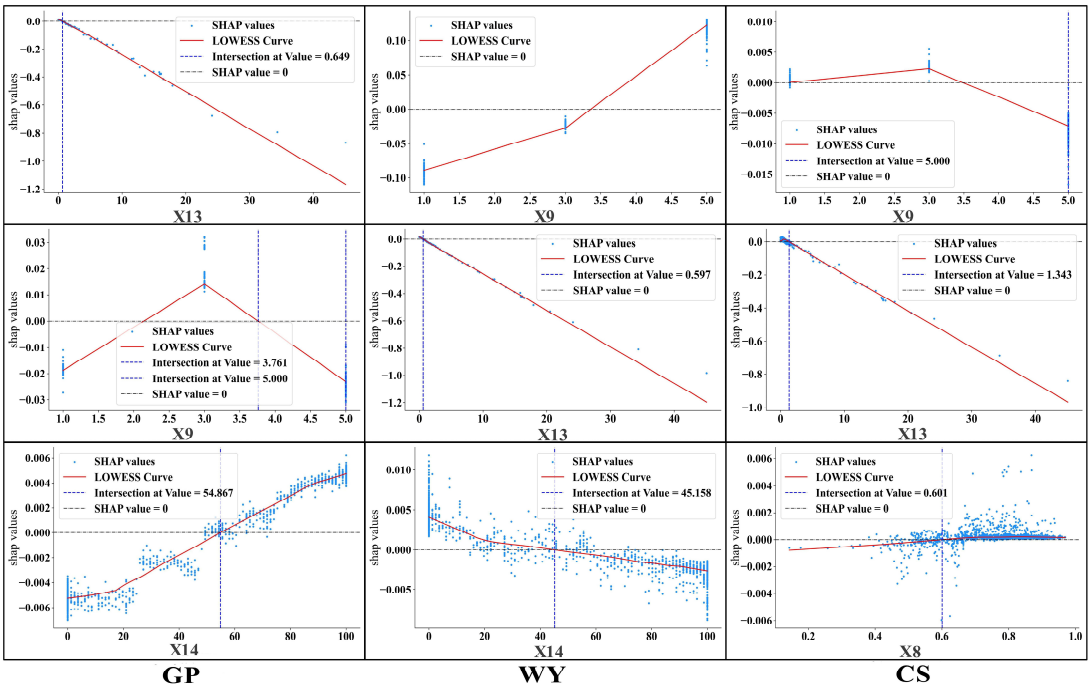


Figure 12. SHAP dependence plots for the three key driving factors of ES balance in the MT region.

Human activity factors showed significant differences in the direction and intensity of their impact on the ESDR of different services. The impact of X9 on GP_ESDR exhibits a nonlinear effect, with increasing land use intensity initially inhibiting, then promoting, and finally inhibiting again. This suggests that appropriate land development can facilitate GP supply–demand balance through the optimization of agricultural patterns, whereas, conversely, overdevelopment is likely to undermine it. Its impact on WY service showed a

continuous promotion trend, indicating that the increase in land use intensity promotes the generation of surface runoff by changing the hydrological process of the underlying surface, thereby alleviating the imbalance between supply and demand of water resources. For the supply–demand of CS service, it showed a continuous inhibition effect, demonstrating that high-intensity human activities weaken the carbon sequestration capacity of ecosystems; in addition, high-intensity land use is generally accompanied by large amounts of carbon emissions, which further deteriorate the balance between supply and demand of CS. The X13 exhibited a linear inhibition effect on the supply–demand of all three ESs, because areas with concentrated populations face increased pressure from grain demand, domestic and production water consumption, and carbon emissions, which exacerbate the supply–demand contradictions of GP, WY, and CS from the demand side. The X14 showed a non-linear response of high-threshold promotion to the supply–demand of GP service, in MT areas, when the proportion of irrigated farmland exceeded 55% (the threshold was 72% in NMT areas), the SHAP value turned from negative to positive and increased, reflecting that sufficient irrigation water is one of the core guarantees for grain yield in arid farmlands in northern China. Correspondingly, in MT areas, the X14 replaced X4 as one of the key driving factors affecting the supply–demand of WY service, showing a high-threshold inhibition response; high proportions of irrigated farmland increase the demand for water resources through large-scale artificial water extraction for irrigation.

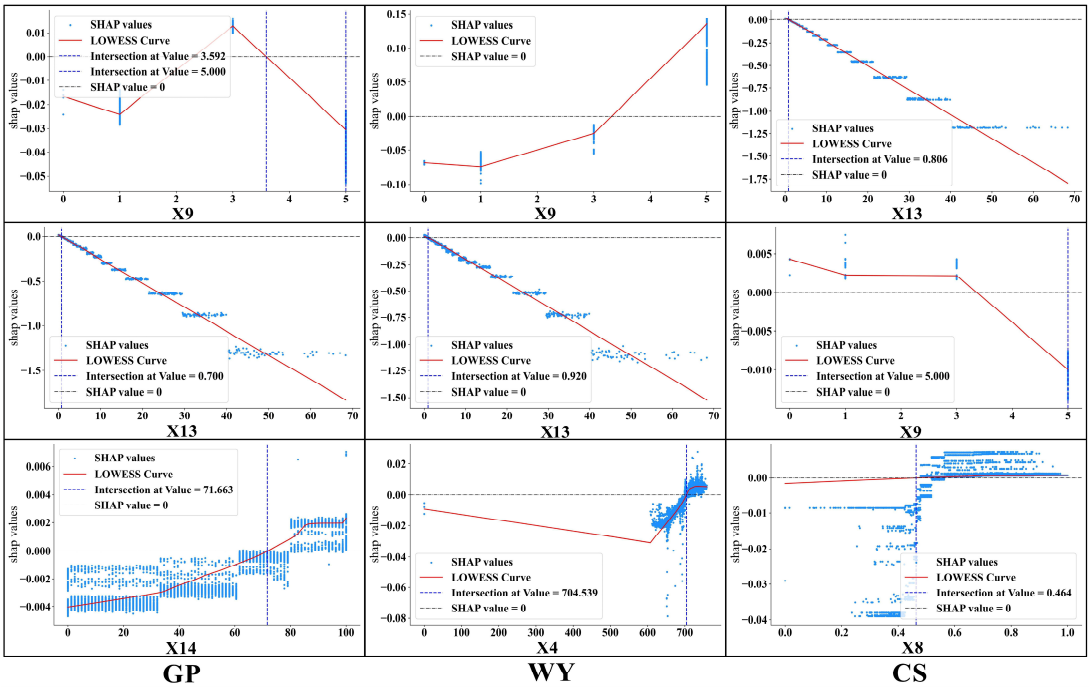


Figure 13. SHAP dependence plots for the three key driving factors of ES balance in the NMT region.

Natural environment factors (X4, X8) had more targeted driving effects on specific services. Among them, X4 only showed a significant effect on the WY service in NMT areas, presenting a non-linear response of high-threshold promotion, when the annual precipitation exceeded 700 mm, the SHAP value quickly turned from negative to positive, indicating that precipitation is the core source on the supply side of WY, and the improvement of WY capacity under high precipitation conditions can directly promote the balance between supply and demand of WY. The X8 only showed a significant effect on CS service, also presenting a high-threshold promotion pattern: the threshold was 0.46 in NMT areas, while it increased to 0.6 in MT areas. This reflects the direct support of NDVI to the supply

side of CS service; higher vegetation coverage leads to stronger CS capacity of ecosystems, which is more conducive to improving the imbalance between supply and demand.

5. Discussion

5.1. Key Characteristics of the ESs Supply Demand Relationship in Typical CGOA

Through a spatio-temporal analysis of ESs supply and demand in the typical CGOA of the Nansi Lake Basin from 2000 to 2020, this study reveals the main patterns of change in the supply and demand of various ESs. Firstly, although GP service showed an overall upward trend and consistently maintained a supply–demand surplus, this was primarily attributable to increased yield per unit area facilitated by factors such as advancements in agricultural technology [62]. Conversely, regional cultivated land area has been continuously shrinking under pressure from urbanization and mineral resource extraction, leading to significant non-agricultural conversion of farmland [63]. Secondly, precipitation is the main source of recharge for surface water resources in the region. However, due to significant interannual fluctuations in precipitation, surface water supply exhibits high instability, with overall supply–demand deficits occurring in 2000, 2005, and 2010. Frequent localized water supply–demand deficits, particularly severe in the western region, highlight the vulnerability of water security and increase the likelihood of dependency on inter-basin water transfers or groundwater over-exploitation [64]. Finally, the imbalance in CS service supply and demand is the most critical. The rapid growth of carbon emissions continues to erode the existing carbon sink surplus [65], with the CS_ESDR index continuously declining and approaching the critical threshold of a supply–demand deficit. If this trend continues, we can boldly predict that the region will exhaust all its carbon sequestration surplus around 2030.

5.2. Differential Impacts of Human Activities on ESs Supply Demand Relationships Under Natural Background Constraints and Carrying Capacity

The spatio-temporal differentiation of ESs supply and demand revealed in this study is essentially the result of the coupling of the regional natural environment background and human activities [66]. The Nansi Lake Basin features flat terrain, fertile soil, and a suitable climate, making it suitable for large-scale agricultural production and concentrated human settlements. Therefore, contiguous farmland concentration areas and block-shaped artificial surfaces interspersed within them are the main landscape types of the region [67]. This pattern is common in most CGOAs in eastern China, such as the Huainan Mining Area and Huaibei Mining Area [68,69]. The supply–demand pattern of ecosystems in NMT areas is mainly affected by urbanization; the rapid expansion of urban boundaries has encroached on a large amount of arable land and ecological space, reducing the potential of grain production and causing the loss of farmland carbon sinks. At the same time, population migration from rural to urban areas and the expanding scale of the urban population have also changed the demand pattern. In contrast, the supply–demand pattern in MT areas is subject to dual pressures from both urbanization and mineral resource development. Underground coal mining activities have exacerbated land subsidence, land loss, hydrological process disruption, and ecosystem degradation, further weakening the supply function of ecosystems [60]. This also confirms the trend observed in this study, where GP_ESDR in the NMT region has surpassed that in the MT region.

5.3. Nonlinear Driving Mechanisms Dominated by Human Activities: An Analysis of ESs Supply Demand Patterns in CGOAs

This study integrates the XGBoost-SHAP model to reveal the complex driving mechanisms behind the supply–demand patterns of ESs in the CGOA. The analysis indicates that human activities are the dominant factor shaping these patterns, with land use intensity

and population density exerting the most significant influence on the ESDR. This confirms that urbanization and population concentration constitute the core pressures leading to regional ecological imbalances [70]. Notably, the driving mechanisms exhibit nonlinearity and threshold effects. For example, the positive impact of irrigated cropland proportion and NDVI on ESs emerges only after reaching certain thresholds, while the influence of land use intensity on grain production fluctuates, with moderate land development being beneficial for improving the GP_ESDR. Furthermore, the unique stress from coal mining subsidence in the MT area clearly reveals the distinct characteristics of driving mechanisms inside versus outside mining zones, emphasizing the importance of mineral resource exploitation as a region-specific driving force [71]. In summary, regional ESs management must acknowledge the dominance of human activities and focus on the nonlinear interactions and spatial heterogeneity of driving factors. For mining-affected areas like MT, targeted measures are urgently needed to remediate the damage caused by coal mining subsidence to the ecological supply side. At the broader regional level, it is essential to optimize land use structure and regulate human activity intensity to synergistically enhance ecosystem sustainability from both the supply and demand sides.

6. Limitations

This study still has certain limitations. First, the MT and NMT areas were compared and analyzed as a precondition based on the status of mineral resource development, but this zoning approach is relatively crude and relies on the researchers' own experience. No spatial clustering methods or comprehensive indicator systems were used to conduct objective ecological management zoning. Second, there are limitations in the scale and accuracy of data: downscaling of multi-source socioeconomic data will inevitably introduce errors, and CE data rely on the population quota method, making it difficult to capture the characteristics of concentrated emissions from industrial production. Third, the coverage of service types is limited: only the GP_ESDM, WY_ESDM, and CS_ESDM sequestration was analyzed, and other types of ESs were not included for a comprehensive assessment.

Future research can be improved in three aspects: First, optimize the zoning method by constructing an objective zoning system combining indicators such as territorial spatial planning, mineral resource development plans, ecological vulnerability, and ecological resilience to lay a foundation for differentiated management. Second, explore and integrate high-resolution, long-time-series earth observation data and socioeconomic statistics, improve existing assessment methods, and calibrate model parameters to enhance the accuracy of supply–demand quantification. Third, expand the types of ESs for assessment, explore the spatial transmission processes of ESs, deepen research on cross-regional supply–demand coordination mechanisms and ecological compensation standards, and provide more comprehensive scientific support for refined ecological management in CGOAs.

7. Conclusions

Taking the CGOAs in eastern China as the research object, this study explored the spatio-temporal evolution laws of ESs supply and demand and differences in driving factors across different element-based zones using comprehensive ESs models and interpretable machine learning algorithms. The results show that there are significant spatio-temporal differentiation characteristics in the supply and demand of regional ESs. GP service maintained a long-term supply surplus, mainly dominated by the Type II ESDM pattern, but the supply surplus potential in MT areas was weaker than that in NMT areas. WY service exhibited significant interannual fluctuations in supply–demand balance, and most regions were in a supply deficit status in most years, mainly characterized by the Type IV ESDM pattern, which reveals the dilemma of regional structural water resource shortage.

The supply surplus of CS service continued to decline due to decreased carbon storage and a surge in carbon emissions; meanwhile, urban built-up areas, as supply–demand deficit areas, expanded year by year, posing a risk of carbon deficit in the future. The driving mechanisms of ESs supply–demand balance in MT and NMT areas share commonalities while also exhibiting significant differences. Human activities are the core driving force shaping the ESs supply–demand pattern, but their impact directions and intensities on different service types are differentiated, and the effects of various factors generally exhibit nonlinear and threshold effects. Additionally, MT areas are significantly affected by coal mining subsidence, indicating that large-scale mineral resource exploitation exacerbates the coordinated pressures among "food security, water resource security, and dual-carbon goals". This study clarifies the dynamic change laws and driving mechanisms of ESs supply and demand in CGOAs, verifies the applicability of the InVEST model and XGBoost-SHAP algorithm, and provides a scientific basis for the optimal allocation of regional natural resources, ecological restoration, and the sustainable development of human-land systems. Future research should address data and model limitations, expand service types, and deepen the simulation of spatial transmission of ESs supply and demand to support more refined ecosystem management.

Author Contributions: Q.N. contributed to the research conception and wrote the major manuscript. D.Z. checked the logical structure of the paper, streamlined some content, and adjusted the format of the paper. Y.W. provided project funding support. Z.D. defined the scope of the coal-grain overlapping areas in this study. G.Q. debugged XGBoost-SHAP using Python and created a graph. All authors have read and agreed to the published version of the manuscript.

Funding: This research was funded by the "2022 CUMT Outstanding Student Innovation Special Fund", Fundamental Research Funds for Central Universities, grant number (2022XSCX36).

Data Availability Statement: The data presented in this study are available upon request from the corresponding author. The data are not publicly available due to privacy.

Acknowledgments: The authors would like to thank the reviewers and the editor, whose suggestions greatly improved the manuscript.

Conflicts of Interest: The authors declare no conflicts of interest.

References

1. Lewis, S.L.; Maslin, M.A. Defining the Anthropocene. *Nature* **2015**, *519*, 171–180. [CrossRef] [PubMed]
2. Liu, C.Q.; Li, S.L.; Liu, X.Y. Biogeochemical Cycles in the Anthropocene and Their Science. *Front. Earth Sci.* **2024**, *31*, 455–466.
3. Shao, W.W.; Zhou, Z.H.; Liu, J.H.; Yang, G.Y.; Wang, J.H.; Xiang, C.Y.; Cao, X.L.; Liu, H.Z. Changing mechanisms of agricultural water use in the urbanization and industrialization of China. *Water Policy* **2017**, *19*, 908–935. [CrossRef]
4. MA (Millennium Ecosystem Assessment). *Ecosystems and Human Well-Being: Current State and Trends: Synthesis*; Island Press: Washington, DC, USA, 2005; pp. 829–838.
5. IPBES (Intergovernmental Science-Policy Platform on Biodiversity and Ecosystem Services). *Global Assessment Report on Biodiversity and Ecosystem Services*; IPBES Secretariat: Bonn, Germany, 2019.
6. United Nations. *Transforming Our World: The 2030 Agenda for Sustainable Development*; United Nations: New York, NY, USA, 2015.
7. Costanza, R.; d'Arge, R.; de Groot, R.; Farber, S.; Grasso, M.; Hannon, B.; Limburg, K.; Naeem, S.; O'Neill, R.V.; Paruelo, J.; et al. The value of the world's ecosystem services and natural capital. *Nature* **1997**, *387*, 253–260.
8. Daily, G.C. Nature's services: Societal dependence on natural ecosystems. *Pac. Conserv. Biol.* **1997**, *6*, 220–221.
9. De Groot, R.S.; Wilson, M.A.; Boumans, R.M.J. A typology for the classification, description and valuation of ecosystem functions, goods and services. *Ecol. Econ.* **2002**, *41*, 393–408. [CrossRef]
10. Hoff, H. Understanding the Nexus. In Proceedings of the Background Paper for the Bonn Conference: The Water, Energy and Food Security Nexus, Bonn, Germany, 16–18 November 2011; Stockholm Environment Institute (SEI): Stockholm, Sweden, 2011.
11. Li, Y.; Zhang, X.; Wang, Q.; Liu, J. Water-energy-food (WEF) nexus efficiency of dynamic slack-based measure in 31 provinces and regions in China. *J. Clean. Prod.* **2024**, *460*, 142433.

12. Zhang, J.; Wang, M.; Liu, K. Social-ecological system sustainability in China from the perspective of supply-demand balance for ecosystem services. *J. Clean. Prod.* **2025**, *497*, 145039.
13. Zhao, H.; Li, C.; Gao, M. Investigation of the Relationship between Supply and Demand of Ecosystem Services and the Influencing Factors in Resource-Based Cities in China. *Sustainability* **2023**, *15*, 7397. [CrossRef]
14. Hu, Z.Q.; Luo, Y.M. Suggestions on environmental quality and food safety in overlapped areas of crop and mineral production. *Sci. Technol. Rev.* **2006**, *26*, 93–94.
15. Hu, Z.Q.; Li, G.S.; Yuan, D.Z. Optimal timing of simultaneous mining and reclamation for coal mining subsidence land in the eastern coal-grain complex area. *J. China Coal Soc.* **2023**, *48*, 373–387.
16. Guo, G.L.; Li, H.Z.; Zha, J.F. Research Status and Countermeasures for Synergistic Development of Coal Mining and Farmland Protection in the Main Coal and Grain Production Composite Zone of the Plain. *Coal Sci. Technol.* **2023**, *51*, 416–426.
17. Xiao, W.; Fu, Y.; Wang, T.; Lv, X. Effects of land use transitions due to underground coal mining on ecosystem services in high groundwater table areas: A case study in the Yanzhou coalfield. *Land Use Policy* **2018**, *71*, 213–221. [CrossRef]
18. Li, S.; Zhao, Y.; Xiao, W.; Yellishetty, M.; Yang, D. Identifying ecosystem service bundles and the spatiotemporal characteristics of trade-offs and synergies in coal mining areas with a high groundwater table. *Sci. Total Environ.* **2022**, *807*, 151036.
19. Shi, Y.; Shi, D.; Zhou, L.; Fang, R. Identification of ecosystem services supply and demand areas and simulation of ecosystem service flows in shanghai. *Ecol. Indic.* **2020**, *115*, 106418. [CrossRef]
20. Burkhard, B.; Kroll, F.; Nedkov, S.; Müller, F. Mapping ecosystem service supply, demand and budgets. *Ecol. Indic.* **2012**, *21*, 17–29. [CrossRef]
21. Villamagna, A.M.; Angermeier, P.L.; Bennett, E.M. Capacity, pressure, demand, and flow: A conceptual framework for analyzing ecosystem service provision and delivery. *Ecol. Complex.* **2013**, *15*, 114–121. [CrossRef]
22. Wolff, S.; Schulp, C.J.E.; Verburg, P.H. Mapping ecosystem services demand: A review of current research and future perspectives. *Ecol. Indic.* **2015**, *55*, 159–171. [CrossRef]
23. Mehring, M.; Ott, E.; Hummel, D. Ecosystem services supply and demand assessment: Why social-ecological dynamics matter. *Ecosyst. Serv.* **2018**, *30*, 124–125. [CrossRef]
24. Gao, M.W.; Hu, Y.C.; Liu, X.Y.; Liang, M.Y. Revealing multi-scale characteristics of ecosystem services supply and demand imbalance to enhance refined ecosystem management in China. *Ecol. Indic.* **2025**, *170*, 112971.
25. Fonseca, F.N.D.A.; Bustamante, M.M.D.C. The importance of indigenous territories for the provision of ecosystem services: A case study in the Brazilian Cerrado-Amazon Transition. *Ecosyst. Serv.* **2025**, *72*, 101706. [CrossRef]
26. Hou, Y.; Liu, Y.; Zeng, H. Assessment of urban ecosystem condition and ecosystem services in Shenzhen based on the MAES analysis framework. *Ecol. Indic.* **2023**, *155*, 110962. [CrossRef]
27. Zhu, X.; Qie, R.; Luo, C.; Zhang, W. Assessment and Driving Factors of Wetland Ecosystem Service Function in Northeast China Based on InVEST-PLUS Model. *Water* **2024**, *16*, 2153.
28. Elleaume, N.; Locatelli, B.; Makowski, D. Uncertainties in future ecosystem services under land and climate scenarios: The case of erosion in the Alps. *Ecol. Model.* **2025**, *502*, 111041. [CrossRef]
29. Xu, J.; Jiang, X.; Liu, H. Monitoring of spatiotemporal changes in ecosystem service functions and analysis of influencing factors in Pingtan Island. *Ecol. Indic.* **2024**, *158*, 111590. [CrossRef]
30. Gwal, S.; Gupta, S.; Sena, D.R. Geospatial modeling of hydrological ecosystem services in an ungauged upper Yamuna catchment using SWAT. *Ecol. Inform.* **2023**, *78*, 102335. [CrossRef]
31. Talukdar, S.; Singha, P.; Mahato, S.; Praveen, B.; Rahman, A. Dynamics of ecosystem services (ESs) in response to land use land cover (LU/LC) changes in the lower Gangetic plain of India. *Ecol. Indic.* **2020**, *112*, 106121. [CrossRef]
32. Meng, Q.X.; Zhang, L.K.; Wei, H.J. Spatiotemporal Evolution of Supply and Demand Risks for Ecosystem Services in the Yi River Basin: A Land Use and Cover Change Perspective. *Acta Ecol. Sin.* **2022**, *42*, 2033–2049.
33. Guo, C.Q.; Xu, X.B.; Shu, Q. Advances in the methodology for evaluating ecosystem service supply and demand. *Acta Ecol. Sin.* **2020**, *39*, 2086–2096.
34. Li, Y.; Liu, Z.; Li, S.; Li, X.; Wang, W. Spatiotemporal Patterning and Matching of Ecosystem Services' Supply and Demand in Changchun, China. *Land* **2023**, *12*, 2101. [CrossRef]
35. Yu, Y.Y.; Li, J.; Han, L.Q.; Zhang, S.J. Research on ecological compensation based on the supply and demand of ecosystem services in the Qinling-Daba Mountains. *Ecol. Indic.* **2023**, *154*, 110687. [CrossRef]
36. Fu, B.J.; Yu, D.D.; Lü, N. China Biodiversity and Ecosystem Services Assessment Index System. *Acta Ecol. Sin.* **2017**, *37*, 341–348.
37. Chen, Y.R.; Qiao, X.N.; Yang, Y.J.; Zheng, J.C.; Dai, Y.L.; Zhang, J. Identifying the spatial relationships and drivers of ecosystem service supply-demand matching: A case of Yiluo River Basin. *Ecol. Indic.* **2024**, *163*, 112122.
38. Liu, H.; Xiao, W.; Zhu, J.; Zeng, L.; Li, Q. Urbanization Intensifies the Mismatch between the Supply and Demand of Regional Ecosystem Services: A Large-Scale Case of the Yangtze River Economic Belt in China. *Remote Sens.* **2022**, *14*, 5147.
39. Zhang, P.; Xu, X.K.; Yang, W.T.; Li, Y.M.; Yao, S.Q. Supply-Demand risk assessment of urban flood resilience from the perspective of the ecosystem services: A case study in Nanjing, China. *Ecol. Indic.* **2025**, *173*, 113397. [CrossRef]

40. Fan, S.X.; Yan, M.; Yu, L.F.; Chen, B.W.; Zhang, L. Integrating ecosystem service supply-demand and ecological risk assessment for urban planning: A case study in Beijing, China. *Ecol. Indic.* **2024**, *161*, 111950. [CrossRef]
41. Galacho-Jiménez, F.B.; Reyes-Corredera, S. Spatial Analysis Model for the Evaluation of the Territorial Adequacy of the Urban Process in Coastal Areas. *Land* **2024**, *13*, 109. [CrossRef]
42. Liu, D.Y.; Dong, W.Z.; Gou, R. Analysis of the Temporal-Spatial Evolution and Driving Factors of Ecosystem Services Supply and Demand in Chongqing: A Study Using InVEST Model and XGBoost-SHAP. *Environ. Sci.* **2025**, 1–17. [CrossRef]
43. Jiang, X.; Wang, B.; Fang, Q.; Bai, P.; Guo, T.; Wu, Q. Ecological Zoning Management Strategies in China: A Perspective of Ecosystem Services Supply and Demand. *Land* **2024**, *13*, 1112. [CrossRef]
44. Shen, J.S.; Li, S.C.; Wang, H.; Wu, S.Y. Understanding the spatial relationships and drivers of ecosystem service supply-demand mismatches towards spatially-targeted management of social-ecological system. *J. Clean. Prod.* **2023**, *383*, 138842. [CrossRef]
45. Xue, Z.J.; Meng, X.W.; Liu, B. Spatio-temporal evolution and driving factors of ecosystem services in the upper Fenhe watershed, China. *Ecol. Indic.* **2024**, *160*, 111803. [CrossRef]
46. Feng, Q.; Duan, B.L.; Zhang, X. Relationship between ecosystem-services trade-offs and supply-demand balance along a precipitation gradient: A case study in the central Loess Plateau of China. *Land* **2024**, *13*, 1057.
47. Zhao, H.; Liu, Q.; Zhang, M. Analysis of Spatial Patterns and Driving Factors of Beijing's Ecosystem Services Using XGBoost-SHAP Model. *Environ. Sci.* **2025**, 1–16. [CrossRef]
48. Zhang, Y.H.; Li, J.; Wang, C. Identification and attribution analysis of integrated ecological zones based on the XGBoost-SHAP model: A case study of Chengdu, China. *J. Environ. Manag.* **2024**, *132*, 106231.
49. Zhang, T.J.; Zhang, S.P.; Cao, Q. The spatiotemporal dynamics of ecosystem services bundles and the socialeconomic-ecological drivers in the Yellow River Delta region. *Ecol. Indic.* **2022**, *135*, 108573. [CrossRef]
50. Liu, J.X.; Wen, C.X.; Liu, Z.W.; Yu, Y. From isolation to linkage: Holistic insights into ecological risk induced by land use change. *Land Use Policy* **2024**, *140*, 107116. [CrossRef]
51. Chen, T.Q.; Guestrin, C. XGBoost: A scalable tree boosting system. In Proceedings of the 22nd ACM SIGKDD International Conference on Knowledge Discovery and Data Mining, San Francisco, CA, USA, 13–17 August 2016; ACM: New York, NY, USA, 2016; pp. 785–794.
52. Lundberg, S.M.; Lee, S.I. A unified approach to interpreting model predictions. In Proceedings of the 31st International Conference on Neural Information Processing Systems, Long Beach, CA, USA, 4–9 December 2017; pp. 4768–4777.
53. Lundberg, S.M.; Erion, G.; Chen, H.; DeGrave, A.; Prutkin, J.M.; Nair, B.; Katz, R.; Himmelfarb, J.; Bansal, N.; Lee, S.I. From local explanations to global understanding with explainable AI for trees. *Nat. Mach. Intell.* **2020**, *2*, 56–67. [CrossRef]
54. Li, Z.Q. Extracting spatial effects from machine learning model using local interpretation method: An example of SHAP and XGBoost. *Comput. Environ. Urban Syst.* **2022**, *96*, 101845. [CrossRef]
55. Lin, Z.A.; Zhao, B.Q.; Meng, Q.G. Characteristic analysis of changes in the planting industry structure and agricultural input-output in the Nansi Lake Basin of China. *Crops* **2007**, *5*, 7–11.
56. Li, Y.; Zhang, Y.; Zhou, J. Study on carbon storage evolution and scenario response under multi-pathway drivers in high-groundwater-level coal resource-based cities: A case study of three cities in Shandong, China. *Land* **2025**, *14*, 2001.
57. Panek, E.; Gozdowski, D. Analysis of relationship between cereal yield and NDVI for selected regions of Central Europe based on MODIS satellite data. *Remote Sens. Appl. Soc. Environ.* **2020**, *17*, 100286. [CrossRef]
58. Sposito, G. Understanding the Budyko equation. *Water* **2017**, *9*, 236. [CrossRef]
59. Wang, D.; Jing, Y.D.; Han, S.M. Analysis of the spatiotemporal relationship between land use carbon emissions and ecosystem service values in the Nan Si Lake Basin based on a gridded approach. *Acta Ecol. Sin.* **2022**, *42*, 9604–9614.
60. Han, J.; Hu, Z.; Mao, Z.; Li, G.; Liu, S.; Yuan, D.; Guo, J. How to Account for Changes in Carbon Storage from Coal Mining and Reclamation in Eastern China? Taking Yanzhou Coalfield as an Example to Simulate and Estimate. *Remote Sens.* **2022**, *14*, 2014. [CrossRef]
61. Li, Y.G.; Liu, W.; Zhu, M.; Feng, Q. Influencing Factors and Paths of the Coupling Relationship Between Ecosystem Services Supply–Demand and Human Well-Being in the Hexi Regions, Northwest China. *Remote Sens.* **2025**, *17*, 1787.
62. Chandio, A.A.; Ozdemir, D.; Jiang, Y. Modelling the impact of climate change and advanced agricultural technologies on grain output: Recent evidence from China. *Ecol. Model.* **2023**, *485*, 110501. [CrossRef]
63. Li, Z.; Ding, M.; Xie, K.; Li, J.; Chen, L. Spatio-temporal characteristics of farmland occupation of construction land expansion and its spatial relationship with grain yield in China for 2000–2020. *J. Geogr. Sci.* **2024**, *34*, 855–870. [CrossRef]
64. Shu, R.; Cao, X.; Wu, M. Clarifying regional water scarcity in agriculture based on the theory of blue, green and grey water footprints. *Water Resour. Manag.* **2021**, *35*, 1101–1118. [CrossRef]
65. Wang, Q.; Xiao, Y. Has Urban Construction Land Achieved Low-Carbon Sustainable Development? A Case Study of North China Plain, China. *Sustainability* **2022**, *14*, 9434. [CrossRef]
66. Bai, Y.; Ochuodho, T.O.; Yang, J.; Agyeman, D.A. Bundles and hotspots of multiple ecosystem services for optimized land management in Kentucky, United States. *Land* **2021**, *10*, 69. [CrossRef]

67. Zhang, W.; Sun, X.; Zhou, J. Ecological function zoning of Nansi Lake Basin in China based on ecosystem service bundles. *Environ. Sci. Pollut. Res.* **2023**, *30*, 77343–77357. [CrossRef]
68. Wang, X.; Han, J.; Lin, J. Response of Land Use and Net Primary Productivity to Coal Mining: A Case Study of Huainan City and Its Mining Areas. *Land* **2022**, *11*, 973. [CrossRef]
69. Hou, Y.; Chang, J.; Yang, Y.; Yao, Y. Research on the Characteristics and Influencing Factors of Spatial Integration of Resource-Based Coal Cities-A Case Study of the Central Urban Area of Huaibei. *Sustainability* **2025**, *17*, 6024. [CrossRef]
70. Zhao, H.; Zhang, X.; Lu, W.; Wei, C.; He, D.; Lei, Y.; Borowiak, K. Spatiotemporal Changes and Driving Mechanisms of Ecosystem Service Supply–Demand Contradictions Under Urbanization. *Land* **2024**, *13*, 1884. [CrossRef]
71. Bao, X.; Guo, Q.; Wu, S.; Luo, J.; Xu, J. Identifying the spatio-temporal evolution and driving mechanisms of ecosystem service value in high groundwater table coal mining areas. *Environ. Monit. Assess.* **2025**, *197*, 581. [CrossRef]

Disclaimer/Publisher's Note: The statements, opinions and data contained in all publications are solely those of the individual author(s) and contributor(s) and not of MDPI and/or the editor(s). MDPI and/or the editor(s) disclaim responsibility for any injury to people or property resulting from any ideas, methods, instructions or products referred to in the content.